EPR spectra and crystal field of hexamer rare-earth clusters in fluorites

S. A. Kazanskii and A. I. Ryskin
S. I. Vavilov State Optical Institute, 12 Birzhevaya Line, 199034 St. Petersburg, Russia

A. E. Nikiforov, A. Yu. Zaharov, and M. Yu. Ougrumov
Ural State University, 51 Prospekt Lenina, 620083 Ekaterinburg, Russia

G. S. Shakurov
Kazan Physical-Technical Institute, 10/7 Sibirsky trakt, 420029 Kazan, Russia
(Received 7 April 2005; published 27 July 2005)

Disordered fluorite-related solid solutions $(AF_2)_{1-x-y}$ $(Ln'F_3)_x$ $(Ln''F_3)_y$, where A=Ca, Sr, Ba; Ln'=Er, Tm, Yb; Ln''=Lu, Y; and $x \ll y = 0.001-0.4$, were studied by both optical detection and conventional electron paramagnetic resonance (EPR) techniques. The EPR spectra of paramagnetic rare-earth ions Er^{3+}, Tm^{3+}, and Yb^{3+} in clusters of diamagnetic Y^{3+} and Lu^{3+} ions were recorded. It appears that the crystalline electric field at the sites of Ln ions in the clusters is of "nearly" tetragonal symmetry and provides for high values of factors $g_{\|}$, approaching the theoretical limits, and small values of factors $g_{\perp} \sim 0$ in the ground states of the paramagnetic Ln ions. It was assumed that all the clusters of Ln ions in the solid solutions appear to be similar in structure to the hexameric clusters, which are the basic structural units of the homologous series of fluorite-related superstructures $(AF_2)_{1-y}(LnF_3)_y$ with compositions $y=5/m$, where m is an integer in the range of 13–19. The structure of "symmetric" hexameric clusters in CaF_2, SrF_2, and BaF_2 hosts was established by computer simulation. The crystalline electric field and the spectroscopic ground-state parameters for Er^{3+}, Tm^{3+}, and Yb^{3+} ions in the hexameric clusters were calculated and found to be in agreement with the experimental data, being totally different from those known for the "isolated" simple cubic and tetragonal centers in the fluorite crystals.

DOI: 10.1103/PhysRevB.72.014127 PACS number(s): 76.30.−v, 75.10.Dg, 61.46.+w, 61.72.Bb

I. INTRODUCTION

Alkaline-earth fluoride crystals AF_2 (A=Ca, Sr, Ba) have a simple fluorite cubic lattice (space group $Fm\bar{3}m$), which can be presented as an infinite sequence of fluorine cubes with every other (alternate) of their central positions occupied by cations. These crystals can be readily doped with trivalent rare-earth ions and yttrium.[1] (Below, these ions will be referred to as Ln ions.) The excess impurity charge (+1) of Ln cations is compensated by embedding additional F^- ions in the anion sublattice interstices. For low dopant concentrations (~0.01 mol % and less), simple tetragonal and/or trigonal centers with local charge compensation (Ln^{3+}-F^-) and simple cubic centers with nonlocal charge compensation (Ln^{3+}) are formed in the fluorite lattice. Higher dopant concentrations favor the formation of pair centers $(Ln^{3+}\text{-}F^-)_2$ and clusters of Ln^{3+} and F^- ions.[1,2]

The Ln trifluorides exhibit a giant, up to about 40 mol %, solubility in alkaline-earth fluorides. An x-ray study shows that nonstoichiometric fluorite-related solid solutions crystallize as the high-temperature cubic α phase, with the cations keeping their crystallographic positions unchanged, while the anion excess gives rise to the formation of disordered defects in the anion sublattice.

Neutron scattering[3–5] and extended x-ray absorption fine structure[6,7] (EXAFS) measurements made it possible to assume more than 20 cluster models.[3–10] The best known ones are the clusters 2:2:2 and 3:4:2, where the notation $l:m:n$ denotes the number of vacancies V_F and interstitial ions F' $(1/2,u,u;u=0.37)$ and F'' $(v,v,v;v=0.41)$ in the anion sublattice.[8,9] These hypothetical models were used to explain some specific features observed in the ionic conductivity,[11,12] dielectric losses,[13] etc., in doped fluorites. The structural stability of some cluster models was confirmed by calculations of Catlow and co-workers.[7–9]

The x-ray[14] and electron diffraction[15] studies revealed a superstructural lattice ordering of the nonstoichiometric fluorite-related solid solutions $A_{1-y}Ln_yF_{2+y}$ with compositions $y=5/m$, where m is an integer in the range of 13–19, prepared under some specific conditions. The superstructures were found in CaF_2 solid solutions with the trifluorides of $Dy \leftrightarrow Lu, Y$ (as well as in *tveitite*, a natural yttrofluorite mineral), SrF_2 doped with the trifluorides of $Eu \leftrightarrow Lu, Y$, and in BaF_2 doped with the trifluorides of the whole Ln series except La.[15–19] The basic structural motif of these superstructures is the hexameric cluster of Ln_6F_{37} type, or 8:12:1 in terms of the above notation. It is actually identical with the Ca_6F_{32} structural unit of the fluorite lattice, in both volume and shape. Therefore, such clusters are readily incorporated into the fluorite lattice accommodating the anion excess (see Fig. 1). In the hexameric cluster, six corner-sharing antiprisms enclose a cuboctahedron of anions F_{12}, which contains one more off-center F^- ion in its cavity.

There are two homologous series of the superstructures. The first one is a completely cation-ordered structure with six trivalent cations in each Ln_6F_{37} cluster and the interstitial anions randomly distributed over the remaining "cubic" parent structure of the fluorite. The other one is a completely anion-ordered structure with one divalent and five trivalent

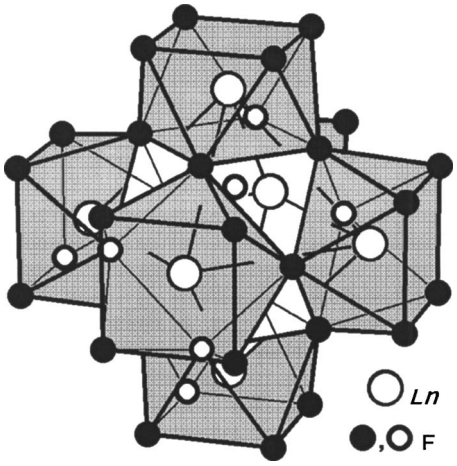

FIG. 1. Hexameric cluster Ln_6F_{37} with inner F_{12+1} cuboctahedron, which replaces the structural unit Ca_6F_{32} with an inner F_8 cube in the fluorite crystal lattice.

cations randomly distributed over the ALn_5F_{37} clusters. While the value of the index m for the observed superstructures corresponds to solid solutions with a comparatively high molar content of LnF_3, from 26 to 43 mol %, domains of the superstructure phases with a high LnF_3 content were also found in less concentrated CaF_2 solid solutions with 5 mol % YF_3.[15]

The EXAFS studies[7,20] show that the disordered fluorite-related solid solutions with a high concentration of LnF_3 can contain the same hexameric clusters that were found in the superstructures. However, in CaF_2—LnF_3 solid solutions, the 8:12:1 clusters are gradually replaced by the 1:0:3 clusters as the ionic radius increases from that of Lu to La.[3,4] It should be noted, however, that the straightforward determination of the cluster structure in a disordered system by x-ray or electron diffraction methods is impossible.

It is well known[1] that detailed information on the structure of impurity centers in crystals can be obtained by electron paramagnetic resonance (EPR). However, the EPR spectra of clusters had not been observed.[1,21] At the same time, clusters of Ln ions were reliably identified by their optical absorption spectra in the spectral range of the $4f$-$4f$ electron transitions in Ln ions.[2,22,23] Furthermore, at dopant concentration of ~1 mol % and higher, the optical spectra of Ln-doped fluorite crystals predominantly exhibit the absorption bands of cluster ions.[24] The optical detection (OD) technique, which involves monitoring the circular dichroism of the optical absorption bands of Ln ions in the external magnetic field, was used in Refs. 24–26 to record the EPR spectra of Ln ions in clusters. The results obtained by the optical detection technique for Er^{3+}, Tm^{3+}, and Yb^{3+} ions in clusters are discussed in Sec. III. (Some distinctive features of the crystal studied are presented in Sec. II.) The experimental data on conventional EPR of Tm^{3+} ions in clusters in CaF_2 are reported in Sec. IV. In Sec. V, the shell theory and exchange charge model are used for calculation of the crystalline electric field and the spectroscopic parameters of the ground states of Er^{3+}, Tm^{3+}, and Yb^{3+} ions in clusters of the Ln_6F_{37} type. The results of this study are briefly summarized in Sec. VI.

II. CRYSTALS

The crystals were grown by the Stockbarger-Bridgman method in graphite crucibles in an apparatus with graphite heaters. Oxygen was removed from source materials of high purity by overheating them in a mixture with a small amount of PbF_2. The melt was used for the crystal growth. Before that, a small amount of PbF_2 was also added to the charge.

The OD EPR study (see Sec. III) was carried out with "fresh" crystal samples. The spectra thereby obtained, as well as those recorded by the conventional EPR, did not reveal the oxygen-compensated paramagnetic Ln^{3+} centers. However, rather intense EPR signals of trigonal Ln^{3+}-O^{2-} centers were recorded in the "aged" samples. Hence, after a long-term storage (of about 20 years), the samples absorbed oxygen.

All the fluorite samples doped with about 1 mol % or more Ln ions are imperfect single crystals. Their cleavage surfaces are slightly mosaic, and each sample consists of a great number of small mutually penetrating crystallites ("microblocks"). The latter fact was revealed by an EPR and x-ray study (see Sec. IV). This is likely to occur due to local distortions of the crystal lattice of these "nanostructural" materials, which may contain regions enriched in Ln^{3+} (aggregates of clusters) embedded into the "unperturbed" fluorite lattice depleted of LnF_3.[27] However, from any crystal, even of highly concentrated solid solution, one could break off samples with "rather flat" cleavage surfaces. After treatment, such samples were used in the experiments.

III. OD EPR SPECTRA OF Er^{3+}, Tm^{3+}, AND Yb^{3+} IONS IN CLUSTERS

The optical detection of EPR by measuring the magnetic circular dichroism[24,28,29] (MCD) is performed in the absorption bands of the paramagnetic centers under study. This allows for finding correlation between the EPR and optical spectra of the same centers. The measuring signal is detected in the optical channel, which is independent of the microwave channel of excitation transitions between the spin levels of an impurity in the magnetic field. This makes it possible to induce "forbidden" transitions (in the case of the factor $g_\perp \sim 0$) at a high microwave power and to use low-quality microwave resonators with volume samples. All these advantages of the OD method were used in our work.

MCD is the difference ($\Delta\chi$) in the absorption coefficients (χ) of a sample in magnetic field $\mathbf{B}_0$ for right- (σ_+) and left- (σ_-) circularly polarized light propagating along $\mathbf{B}_0$:

$$\Delta\chi = \chi(\sigma_+) - \chi(\sigma_-). \quad (1)$$

Without the magnetic field, $\Delta\chi=0$, because the absorption coefficients for right- and left-circularly polarized light are equal. When $\mathbf{B}_0$ is switched on, the ground state of a paramagnetic impurity splits. At a low temperature, the Boltzmann population of the Zeeman sublevels of the ground states induces MCD—that is, $\Delta\chi \neq 0$ so far as optical transitions from the different sublevels to the upper states commonly have different circular polarization. As a rule, the Zeeman splitting is much less than the bandwidth of the optical

absorption bands. In this case, the dependence of MCD on the magnetic field, $\Delta\chi(\mathbf{B}_0)$, is a function of only the populations of the sublevels, which can be described by the Brillouin function for the magnetization of a paramagnet.[30] For the effective spin $S=\frac{1}{2}$ in the ground state of a paramagnetic impurity, this reads

$$\Delta\chi(B_0) = \Delta\chi^{\max} \tanh(g\mu_B B_0/2k_B T), \tag{2}$$

where g is the spectroscopic splitting factor, μ_B is the Bohr magneton, k_B is the Boltzmann constant, and $\Delta\chi^{\max} \equiv \Delta\chi^{\max}(\lambda)$ is the saturation value of MCD, $\Delta\chi$, recorded with probe light at the given wavelength λ in high magnetic fields. If the sample is also exposed to a microwave field of frequency ν_1, which induces transitions between the Zeeman sublevels of the ground state at a resonant value of the magnetic field, the dependence $\Delta\chi(B_0)$ will have a dip. The change in the field dependence of the MCD upon applying the microwave field will represent the OD EPR spectrum:

$$\delta\Delta\chi(B_0) = \Delta\chi(P_1 = 0, B_0) - \Delta\chi(P_1, B_0), \tag{3}$$

where P_1 is the power of the microwave field.

In our OD EPR experiments ($\nu_1 \approx 36$ GHz), a sample (up to $4\times4\times4$ mm^3 in size) was placed in a low-quality microwave resonator with apertures for the probe light beam at a wavelength isolated by a monochromator. The circular polarization modulator periodically changes the polarization of the probe light $\sigma_- \leftrightarrow \sigma_+$. Having passed through the sample, the light arrives at a photodetector. For MCD measurements, the modulation of the light intensity with the change in its circular polarization is recorded. In OD EPR experiments, the modulation of the MCD induced by switching on and off the microwave power is measured.

A study of solid solutions $(AF_2)_{1-x}(Ln'F_3)_x \equiv AF_2:Ln'_x$ (where $Ln' \equiv$ Er, Tm, or Yb and $0.0005 \leqslant x \leqslant 0.02$) at $T=1.8$ K in the external magnetic field revealed a strong MCD of all the optical absorption spectra of $(Ln')^{3+}$ ions in clusters.[24–26] (We studied the optical bands in the visible and near-IR spectral regions.) The MCD observed is very sensitive to the orientation of the crystallographic axes in the magnetic field. This reveals the strong anisotropy of the g tensor ($g_\parallel \gg g_\perp$) of the ground states with an alignment of the principal axis ($g_\parallel$) along the crystal axis $\mathbf{C}_4$. The $g_\parallel$ values [which were determined from the $\Delta\chi(B_0)$ dependences at $\mathbf{B}_0 \| \mathbf{C}_4$] appear to be very close to the maximum theoretical limit for all Ln' ions studied (see below). However, the OD EPR spectra of these solid solutions exhibit broad background absorption with a scarcely discernable structure. These clusters turn out to be magnetically concentrated systems (see below).

In order to suppress the spin-spin interactions between the paramagnetic $(Ln')^{3+}$ ions in clusters, they were diluted (up to 90% and more) by diamagnetic $(Ln'')^{3+}$ ions Lu^{3+} or Y^{3+}. We studied the solid solutions $(AF_2)_{1-x-y}(Ln'F_3)_x(Ln''F_3)_y \equiv AF_2:Ln'_x,Ln''_y$, where $0 \leqslant x \ll y \leqslant 0.4$. The capability of such a dilution follows, for example, from Refs. 22–24. It was shown that the distribution of Ln' and Ln'' ions with close values of ionic radii is statistically independent in clusters. This fact was also confirmed by the OD EPR study at a gradual change in the concentration ratio of paramagnetic and diamagnetic ions in the crystals (see Fig. 2). In the process of the dilution, the initially broad OD EPR band gradually narrowed and exhibited a structure.

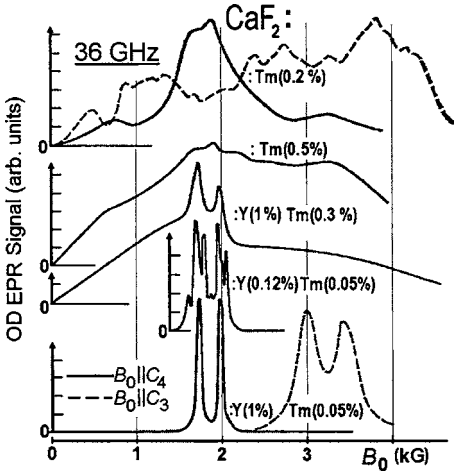

FIG. 2. OD EPR spectra of Tm^{3+} ions in clusters at different concentrations and dilutions of Tm^{3+} ions by diamagnetic Y^{3+} ions in CaF_2. (The spectra were recorded by monitoring $^3H_6 \rightarrow {}^3F_{2,3}$ optical transitions in the $4f$ shell of Tm^{3+} ions in clusters.) Orientations of the crystals in the external magnetic field are $\mathbf{B}_0 \| \mathbf{C}_4$ (solid line) and $\mathbf{B}_0 \| \mathbf{C}_3$ (dashed line). $\nu_1 = 36$ GHz. $T = 1.8$ K.

For all the paramagnetic Ln' ions in the "diluted" clusters, the detailed study of OD EPR and MCD revealed a strong anisotropy of their g tensors ($g_\parallel \gg g_\perp$) with the alignment of their principal axes ($g_\parallel$) along the crystal axes $\mathbf{C}_4$. It was also found that the $g_\parallel$ values do not noticeably change throughout the range of existence of the solid solutions studied at various x and y with either Lu or Y.

Figure 3 depicts the OD EPR spectra ($\nu_1 \sim 36$ GHz) of Er^{3+}, Tm^{3+}, and Yb^{3+} ions in clusters of diamagnetic ions in some fluorite-related solid solutions.

The spectroscopic factors of the paramagnetic Ln' ions in clusters are listed in Table I. It can be seen that factors $g_\parallel$ of

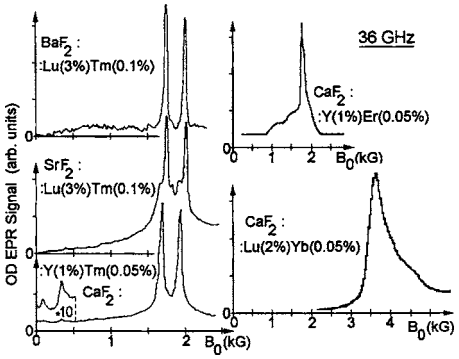

FIG. 3. OD EPR spectra of Tm^{3+}, Er^{3+}, and Yb^{3+} ions embedded in clusters of diamagnetic Lu^{3+} and Y^{3+} ions in fluorite-type crystals. (The spectra were recorded by monitoring the optical transitions $^4I_{15/2} \rightarrow {}^4F_{5/2}$ in Er^{3+}, $^3H_6 \rightarrow {}^3F_{2,3}$ in Tm^{3+}, and $^2F_{7/2} \rightarrow {}^2F_{9/2}$ in Yb^{3+}.) Orientation of the crystals in the external magnetic field is $\mathbf{B}_0 \| \mathbf{C}_4$. $\nu_1 = 36$ GHz. $T = 1.8$ K. Note the different X scales for the Tm^{3+} ion and for the Er^{3+} and Yb^{3+} ions.

TABLE I. Experimental values of spectroscopic splitting factors of paramagnetic ions Ln′=Er^{3+}, Tm^{3+}, and Yb^{3+} embedded in clusters of diamagnetic ions in fluorite-related solid solutions AF_2:Ln''_y (A=Ca, Sr, Ba; Ln″=Y, Lu) and their calculated values.

Ln′ ion	Crystal	Ground doublet	$g_{\parallel}^{\lim}$	Experimental values		Calculated values	
				$g_{\parallel}$	Δ (cm^{-1})	$g_{\parallel}$	Δ (cm^{-1})
Er^{3+}	CaF_2	±15/2	18	15.5±0.3[a]		17.9	
	SrF_2			16±0.5[a]		17.9	
	BaF_2			17.2±0.3[a]		18.0	
Tm^{3+}	CaF_2	±6	14	13.62±0.03[b]	Δ_1=0.20±0.07[b]	13.8	0.9
				13.8±0.3[a]	Δ_1=0.3±0.1[a] Δ_2=2±1[a]		
	SrF_2			13.8±0.3[a]	Δ_1=0.3±0.2[a] $\delta_2 \geqslant 1$[a]	13.8	2.2
	BaF_2			13.8±0.3[a]	Δ=0.2±0.1[a]	13.8	1.9
Yb^{3+}	CaF_2	±7/2	8	6.8±0.2[a]		8.0	
	SrF_2			[c]		7.9	
	BaF_2			[c]		7.9	

[a]OD EPR (ν_1=36 GHz) results for solid solutions in a wide range of y=0.001–0.4: see Sec. III.
[b]EPR data (ν_1=37–100 GHz) for CaF_2:$Y_{0.01}Tm_{0.0005}$: see Sec. IV.
[c]No data available.

the ground states of Er^{3+}, Tm^{3+}, and Yb^{3+} in clusters have the record-high values, which are close to the theoretical limit $g^{\lim}=2Jg_J$, where J is the total angular momentum and g_J is the Lande factor of the lowest multiplet for each of the Ln′ ions.[31] For the $g_{\perp}$ factor, the estimate $g_{\perp} \ll g_{\parallel}$ holds. Hence, the ground states of these ions are approximately pure $|\pm J\rangle$ doublets. These results can be explained by the specific crystal field of the local surrounding of the Ln ions in hexameric clusters (see Sec. V).

It is noteworthy that the EPR lines of Er^{3+} and Yb^{3+} ions in clusters of diamagnetic ions have an appreciable width even in orientation of the external magnetic field $\mathbf{B}_0 \| \mathbf{C}_4$ along the principal axis of the g tensor (see Fig. 3). In contrast, the EPR spectra of Tm^{3+} exhibit rather narrow lines of the characteristic doublet due to the hyperfine interaction of the electron shell of $(^{169}Tm)^{3+}$ with its nuclear spin I=1/2 (the isotope abundance of ^{169}Tm is equal to 100%). The spacing between the lines in the Tm^{3+} doublets (from 240 to 245 G in the $\mathbf{B}_0 \| \mathbf{C}_4$ orientation) is approximately the same for all solid solutions. This is governed by the hyperfine interaction constant $A_{\parallel}$ (see Sec. IV for details). Depending on the cation of a fluorite crystal lattice (Ca, Sr, or Ba), the diamagnetic ions that form clusters (Lu or Y), and on the specifics of the crystal growth, the OD EPR spectra of Tm^{3+} exhibit either a single or a few close or far away doublets (see Figs. 2 and 3). The presence of a number of Tm^{3+} doublets indicates the existence of a series of possible types of crystallographic positions of Ln ions in the clusters. Each doublet can be characterized by its own value of the initial splitting Δ of the Tm^{3+} ground state in the zero magnetic field (see Sec. IV). In particular, the presence of two weak doublets in the OD EPR spectrum of CaF_2:$Y_{0.01}Tm_{0.0005}$ in low magnetic fields is evidence of the corresponding Tm^{3+} ions having the initial zero-field splitting only slightly less than the energy of a microwave quantum ($\sim$1.2 cm^{-1}).

The orientation of the principal axis ($g_{\parallel}$) of the g tensor along the crystal axis $\mathbf{C}_4$ could be evidence of a pure tetragonal symmetry of a coordination polyhedron of the anions surrounding Ln ions in the clusters. However, the experimental data are evidence of some distortion of the tetragonal symmetry. The width of the EPR lines of the paramagnetic Ln′ ions in the clusters of the diamagnetic Ln″ ions appreciably increases with deviation of the external magnetic field from the principal direction $\mathbf{B}_0 \| \mathbf{C}_4$ (e.g., see the EPR spectra of CaF_2:$Y_{0.01}Tm_{0.0005}$ in Fig. 2). The dependence of this orientational broadening on the angle φ of the direction of the magnetic field $\mathbf{B}_0$ with the crystal axis $\mathbf{C}_4$ turns out to be significantly stronger than the theoretical one, $\sim 1/\cos\varphi$, which could be assumed for an anisotropic g tensor and an inhomogeneous EPR line. Furthermore, the broadening appreciably increases with an increase in the concentration of the solid solutions above $y \sim 0.03$. Therefore, in highly concentrated solid solutions with $y \rightarrow 0.4$, the OD EPR spectrum is observable only in the $\mathbf{B}_0 \| \mathbf{C}_4$ orientation. The orientational broadening can be explained by a misalignment of the principal axes $g_{\parallel}$ with the preferable directions ($\mathbf{C}_4$) in the solid angle $\Omega \leqslant 5°$ for CaF_2 with $y \leqslant 0.02$. For the maximum concentration $y \sim 0.4$, the solid angle is estimated as $\Omega \leqslant 30°$. This value by far exceeds the misalignments of the crystal axes *per se*, which occur because of the existence of a number of mutually penetrating microblocks in the samples studied (see Secs. II and IV).

The OD EPR study demonstrates that the hexameric clusters Ln_6F_{37} are formed in solid solutions. It can be seen from Fig. 1 that all the Ln sites in Ln_6F_{37} clusters are identical and the symmetry of the crystal field at the Ln sites is tetragonal (if the off-center position of the F^- ion in the cavity of the cuboctahedron F_{12} is neglected). A broad background ab-

sorption observed in the OD EPR spectra of the solid solutions, which contain only the paramagnetic Ln′ ions, and their smooth variation with gradual dilution of the paramagnetic ions by the diamagnetic ones show, however, that there are no "isolated" clusters Ln_6F_{37} in the fluorite lattice. The Ln_6F_{37} clusters appear to coagulate, thus forming the domains of Ln-enriched phase in the crystal lattice. Our estimates show that the concentration of Ln in the Ln-enriched phase may be close to the maximum solubility of LnF_3 in fluorites (up to ~40 mol %).

A significant width of the OD EPR lines of Er^{3+} and Yb^{3+} ions in clusters even in low-concentrated solid solutions (~1 mol %) and the presence of a set of the hyperfine doublets in the EPR spectra of Tm^{3+} ions indicate the existence of a number of "slightly" different positions of Ln ions in clusters. This conclusion is in agreement with the investigations performed by optical spectroscopy in doped fluorites.[2] The above facts and also the abnormal orientational broadening of the OD EPR spectra with an increase in the concentration of the solid solutions, apparently, can be explained by the interaction between Ln_6F_{37} clusters and by the absence of the complete order in their arrangement in cluster domains. The formation of clusters and their domains, probably, gives rise to the microblock structure of the solid solutions studied (see Sec. IV). It should be noted that, besides clusters of the Ln_6F_{37} type, the OD EPR spectra do not reveal clusters of other possible types.

IV. EPR OF Tm^{3+} IONS IN HEXAMERIC CLUSTERS

The paramagnetic Ln′ ions in clusters of diamagnetic Ln″ ions were also studied with an E-12 Varian EPR spectrometer (Q band, $\nu_1 \sim 37$ GHz) and an EPR spectrometer with a quasioptical recording channel of the microwave absorption in the frequency range of 65–100 GHz.[32] However, the EPR spectra were reliably detected only for clusters with Tm^{3+} ions. The spectra had rather low intensity and could be observed in crystals with no more than about 5 mol % of $Ln''F_3$. The detailed study was performed on the clusters in CaF_2 crystals.

The dependence of the frequency of resonant transitions on the magnitude of the magnetic field was investigated with the quasioptical EPR spectrometer for crystals $CaF_2:Y_{0.01}Tm_{0.0005}$ (see Fig. 4). In these measurements, the direction of microwave propagation, **k**, was orthogonal to $\mathbf{B}_0$. The EPR spectra were reliably observed only for the orientation of both the oscillating ($\mathbf{B}_1$) and static magnetic fields along the crystal axis $\mathbf{C}_4$. As far as there was no resonator in the spectrometer, we used large $\sim 10 \times 10 \times 10$ mm^3 samples with a number of microblocks (see below). However, for the $\mathbf{B}_0 \| \mathbf{C}_4$ orientation, the spectra from different microblocks merge into a single line.

$CaF_2:Y_{0.01}Tm_{0.0005}$ crystals of $\sim 4 \times 2 \times 0.5$ mm^3 size were studied with the Varian spectrometer. The measurements were aggravated by the appreciable dielectric losses in the samples, which are due to the presence of two-level systems.[33] The dielectric losses made it impossible to study the electric dipole transitions between the levels of non-Kramers doublets of the ground states of Tm^{3+} ions.[31] As for the magnetic dipole transitions, the most intense EPR signals of Tm^{3+} were recorded in the $\mathbf{B}_0 \| \mathbf{B}_1 \| \mathbf{C}_4$ orientation in agreement with the theory.[31]

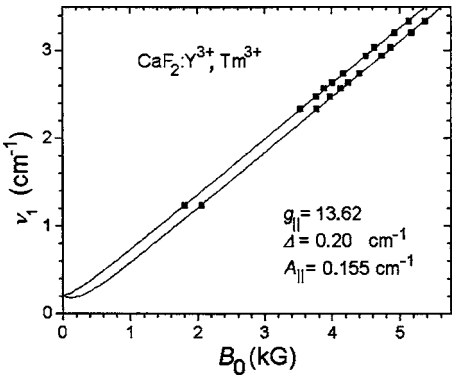

FIG. 4. Resonance frequency of the strongest EPR hyperfine doublet of Tm^{3+} ions embedded in clusters of diamagnetic ions in $CaF_2:Y_{0.01}Tm_{0.0005}$ vs external magnetic field $\mathbf{B}_0$. Experimental data are depicted by points. The solid lines are calculations with $g_\parallel = 13.62$, $A_\parallel = 0.155$ cm^{-1}, and $\Delta = 0.20$ cm^{-1}. Orientation of the crystal in the magnetic fields in $\mathbf{B}_0 \| \mathbf{B}_1 \| \mathbf{C}_4$. $T = 4.2$ K.

Figure 5(a) shows the orientation dependence of the resonance frequencies of $CaF_2:Y_{0.01}Tm_{0.0005}$ for the rotation of $\mathbf{B}_0$ in the (111) plane. Only the low-field hyperfine resonance of Tm^{3+} is presented. The orientation dependence corroborates the existence of the three basic magnetically nonequivalent tetragonal centers in clusters. Figure 5(b) shows the extra splitting of both the low- and high-field hyperfine resonances with an increase in the angle of the magnetic field $\mathbf{B}_0$ with the $\mathbf{C}_4$ axis of the crystal. It may be evidence of a misalignment of the $g_\parallel$ axes with the preferable directions ($\mathbf{C}_4$) within a solid angle of a few degrees. This can also arise from the misalignment of the crystal axes due to the existence of a great number of microblocks in the samples studied.

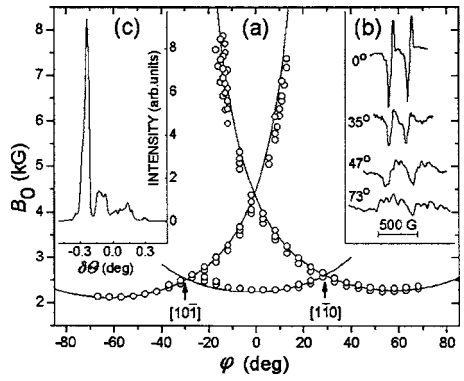

FIG. 5. (a) Orientation dependence of the low-field hyperfine resonance of Tm^{3+} upon rotation of $\mathbf{B}_0$ in the (111) crystal plane of $CaF_2:Y_{0.01}Tm_{0.0005}$, where φ is the angle of $\mathbf{B}_0$ with respect to the $[2\bar{1}\bar{1}]$ direction. The solid lines are calculations, and the circle points are the experimental data. (b) The observed splitting of Tm^{3+} resonances with an increase in the angle of the magnetic field $\mathbf{B}_0$ with $\mathbf{C}_4$ axis of the crystal. (a), (b) $\nu_1 = 37$ GHz, $T = 4.2$ K. (c) Microblock structure of the x-ray diffraction pattern of the (111) reflection (see Sec. IV).

The existence of microblocks was revealed by the x-ray study on the reflections from the cleavage surfaces of the crystals. Figure 5(c) shows a diffraction pattern which exhibits about ten different microblocks on the ($\sim 4 \times 2$ mm^2) surface of the sample studied by EPR [see Fig. 5(a)]. In this experiment, the detector of the x-ray diffractometer was set to record the (111) reflection at an angle of $2\Theta = 35.82°$ (FeK_α). The rotation of a crystal holder, which is usually used for averaging, was switched off. The x-ray diffraction pattern was recorded by subsequent inclination of a crystal with a step of $\delta\Theta = 0.02°$.

The powders prepared from the grown crystals with LnF_3 concentration up to 5 mol % were also studied by the x-ray diffractometry. No splitting or broadening of the x-ray reflections were found in these powders as compared to the powders of pure CaF_2. Hence the studied crystals contain only the cubic α phase. It should be noted that, in concentrated solid solutions (BaF_2 with ~ 25 mol % of LnF_3), the cubic α phase coexists with other distorted cubic phases.[27]

The results of the EPR study were treated under assumption that the non-Kramers doublet of the ground state of Tm^{3+} ion lies far below the other excited Stark levels. Griffith[34] has shown that, in this case, the behavior of the non-Kramers doublet in a magnetic field is determined only by factor $g_\parallel$, whereas $g_\perp = 0$. The spin Hamiltonian for the ground doublet ($S = 1/2, I = 1/2$) is

$$H = \Delta S_x + g_\parallel \mu_B S_z B_{0z} + A_\parallel S_z I_z, \tag{4}$$

where Δ is the zero-magnetic-field splitting of the doublet, $A_\parallel$ is the hyperfine interaction constant, and B_{0z} is the component of the static magnetic field along the $g_\parallel$ direction. From the EPR of $CaF_2:Y_{0.01}Tm_{0.0005}$ measured in the $\mathbf{B}_0 \| \mathbf{C}_4$ orientation, we get $A_\parallel / g_\parallel \mu_B = 244 \pm 2$ G, $g_\parallel = 13.62 \pm 0.03$, and $\Delta = 0.2 \pm 0.07$ cm^{-1}. Using these parameters and taking into account a small deflection $\sim 4°$ of the (111) crystal plane from the plane of rotation of $\mathbf{B}_0$ in the experiment, we calculated the orientation dependence which is shown in Fig. 5(a) by solid lines. In high magnetic fields, these curves go approximately through the centers of gravity of the points corresponding to the extra splitting of Tm^{3+} resonances [see Fig. 5(b)].

Although the presence of microblocks in the samples is proved by the x-ray study, the extra splitting of Tm^{3+} resonances [see Fig. 5(b)] can also be caused by the lowering of the tetragonal symmetry of Ln ions and a corresponding increase in number of the magnetically nonequivalent centers in clusters. This may be brought about by a displacement of a fluorine atom from the center of the cuboctahedron, interactions of the neighboring clusters, etc. (see Sec. III). However, on the basis of our EPR study, we can substantiate only a simplified model of the tetragonal centers of Tm^{3+} ions in the clusters characterized by the only factor $g_\parallel$ and the random misalignment of the crystallographic and/or $g_\parallel$ axes within a solid angle of a few degrees.

V. CRYSTAL FIELD AND GROUND-STATE SPECTROSCOPIC PARAMETERS OF RARE-EARTH IONS IN HEXAMERIC CLUSTERS

The starting point for estimating the crystalline electric field (CEF) in a hexameric cluster is the calculation of the arrangement of atoms inside and outside the cluster. For this purpose, computer simulations[35] can be used. The calculations of some cluster structures in the fluorite lattices were made in Refs. 7–9. However, to determine the CEF parameters for a lanthanide ion in the hexameric cluster, we have to obtain more detailed information on the position of atoms and their induced electrical dipole moments.

Using an approach described in Ref. 36, we have computed the atomic structure of a region of the fluorite crystal lattice with the embedded hexameric cluster. The calculations were made in the framework of a pair-potential approximation coupled with the shell model description of lattice ions.[37] The core and shell equilibrium positions for ions in the defected region were found by minimizing the crystal lattice energy as follows:[35,36]

$$E = \frac{1}{2}\sum_i \sum_{j(\neq i)} V_{ij} + \frac{1}{2}\sum_i k_i |\vec{l}_i|^2, \tag{5}$$

where the first term is the sum over the pair potentials of different ions, the second term is the interaction energy between the core of the ith ion and its shell shifted relative to the core by a displacement vector $\vec{l}_i$, and k_i is the shell-core spring constant.

The pair potential is given by the equation

$$V_{ij} = V_{ij}^* + f_{ij}(|\vec{r}_{ij}|) + g_{ij}(|\vec{r}_{ij} - \vec{l}_i + \vec{l}_j|), \tag{6}$$

where $\vec{r}_{ij}$ is the radius vector between the ion cores and V_{ij}^* is the Coulomb interaction of the ith and jth ions.

The screening of the Coulomb potential due to the overlap of electronic densities of ions can be described by the short-range potential

$$f_{ij}(r) = -A_{ij} \exp(-B_{ij} r)/r. \tag{7}$$

The Born-Mayer repulsion and van der Waals attraction can be written as

$$g_{ij}(r) = C_{ij} \exp(-D_{ij} r) - \lambda_{ij}/r^6. \tag{8}$$

The model parameters for fluorite crystals were previously determined in Ref. 36. The potential parameters of the F^--F^- interaction were obtained from Hartree-Fock calculations of the interaction of two fluorine ions. The parameters of the A^{2+}-F^- short-range repulsive potential were obtained by fitting the calculated crystal properties to the experimental data on the lattice, dielectric and the elastic constants, and the frequencies of Raman- and IR-active vibrational modes for the host fluorite crystals. The parameters of the short-range electrostatic screening were calculated by numerical integration of the free-ion electron densities. The parameters of the Gd^{3+}-F^- short-range potential were found by fitting the calculated results to the electron-nuclear double-resonance (ENDOR) data on the positions of anions around a cubic Gd^{3+} center in the fluorite lattices.

In this work, we used more accurate values of the interaction potentials for Ca- and Sr fluorite crystals. These parameters, as well as the parameter k_i for the Gd^{3+} ion, were calculated to fit also the ENDOR data on low-symmetry centers of Gd^{3+} in the fluorite-type crystals.[38,39] All the potential parameters used in this work along with the charges of ion

TABLE II. The model parameters[a] of interacting ions (in atomic units).

i	j	A_{ij}	B_{ij}	C_{ij}	D_{ij}	λ_{ij}	k_i	X_i	Y_i
Ca^{2+}	F^-	31.720	1.5490	223.532	2.0865		22.1800	8	−6
Sr^{2+}	F^-	75.042	1.5570	261.181	1.9683		10.5741	8	−6
Ba^{2+}	F^-	164.932	1.5575	294.125	1.8414		4.8574	8	−6
F^-	F^-	36.456	1.3778	157.083	1.8927	69.5469	4.1797	5	−6
Gd^{3+}	F^-			267.283	2.058		80.0	11	−8

[a]Only the values of parameters used in the calculations are given.

cores, X_i, and the shells, Y_i, are listed in Table II.[40] Below, we neglect the difference in the Ln^{3+}-F^- pair potentials for the lanthanide ions studied and assume them equal to that of Gd^{3+}-F^-.

The simulation of a crystal structure with the embedded hexameric cluster started with the replacement of the octahedron of the six nearest A^{2+} cations of the fluorite lattice by Ln^{3+} ions. The internal cube of 8 F^- ions was replaced by a cuboctahedron of 12 F^- ions which were located at the middle of the edges of that cube. One more F^- ion was located at the center of the cluster. Other ions occupied the unbiased positions of the AF_2 crystal lattice. Then, with the cubic symmetry of the arrangement fixed, the structure relaxation of the defected region enclosing 250 ions was calculated and the equilibrium positions of atoms and shell-core displacements were determined. The Coulomb interaction between the ions of the defected region and the ions of the rest of the crystal was calculated by the Ewald method.

In all fluorite crystals, the relaxation resulted in a stable configuration of Ln_6F_{37} cluster and surrounding ions. As a result of the relaxation, a F_{12} cuboctahedron grows in size, pulling up to Ln_6 octahedron. Weak distortions of the fluorite lattice are observed up to the border of the defected region (of about 15 spheres from the cluster center). Even distant fluorine ions have noticeable shell-core displacements, acquiring significant electrical dipole moments.

With neglect of a fluorine atom in the cuboctahedron cavity, the eight nearest fluorine ligands around a lanthanide ion form a distorted square antiprism with C_{4v} symmetry (see Fig. 6). The calculated distances and angles in the coordination polyhedron surrounding Ln ion in the "isolated" hexameric cluster are given in Table III.

In CaF_2, the average ⟨Ln-F⟩ distance in the square antiprism was found to be equal to 2.35 Å and the ⟨Ln-Ln⟩ distance between the nearest Ln ions in the hexameric cluster to 4.03 Å. It should be noted that the same ⟨Ln-F⟩ length in the $Ca_{0.9}Er_{0.1}F_{2.1}$ and $Ca_{0.68}Er_{0.32}F_{2.32}$ solid solutions was measured in Refs. 6 and 20 by EXAFS as equal to 2.35 and 2.25 Å and the ⟨Ln-Ln⟩ distance to 4.21 and 4.16 Å, respectively.

The crystal-field Hamiltonian for a lanthanide ion is given by the equation[31,41]

$$H_{CF} = \sum_{p=2,4,6} \sum_{q=0}^{p} B_{pq} O_p^q = \sum_{p=2,4,6} \alpha_p \sum_{q=0}^{p} B_p^q O_p^q, \qquad (9)$$

where α_p are Stevens coefficients, O_p^q are the angular momentum operators, and B_p^q are the parameters determined by the distribution of electrostatic charges of the surroundings.

In this work, we used the exchange charge model[42,43] (ECM). It takes into account the electrostatic fields generated by point charges and dipoles of the neighboring ions, as well as the exchange interaction of the $4f$ shell of the Ln ion with ligand electrons. The B_p^q parameters are the sum of the electrostatic and exchange terms:

$$B_p^q = B_{p\ el}^q + B_{p\ s}^q, \qquad (10)$$

The electrostatic term is

$$B_{p\ el}^q = K_p^q (1-\sigma_p) e^2 \langle r^p \rangle \sum_{\alpha} (-Z_\alpha) P_p^q(x_\alpha, y_\alpha, z_\alpha, r_\alpha) r_\alpha^{-(2p+1)}, \qquad (11)$$

where the summation α is taken over all the cores and shells of the neighboring ions having coordinates $(x_\alpha, y_\alpha, z_\alpha)$ in a fixed Cartesian coordinate system with the center at the $4f$ core of the Ln ion, r_α is the distance from the lanthanide ion to the core or the shell of the ligand, $P_p^q(x_\alpha, y_\alpha, z_\alpha, r_\alpha)$ are homogeneous polynomials of degree p listed in Ref. 31, $\langle r^p \rangle$ is the mean value of r^p averaged over the atomic wave functions for $4f$ electrons,[31] σ_p is the shielding factor which allows for polarization of the closed $5s^2 5p^6$ shells within the Ln ion and its effect on the CEF at the $4f$ core,[44] e is the electron charge, Z_α is the effective charge number which

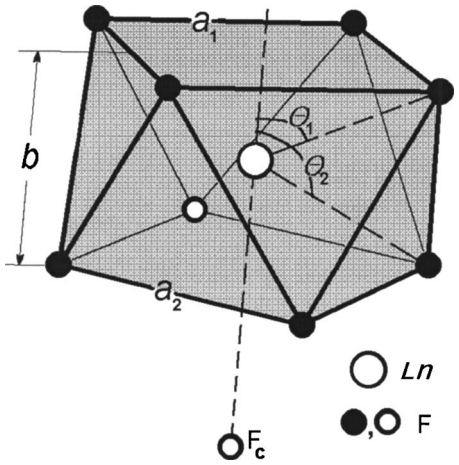

FIG. 6. Coordination polyhedron (8+1) of anions around the Ln ion in the hexameric cluster which was calculated to be a distorted square antiprism ($a_2 > a_1 > b$) with C_{4v} symmetry+atom F_c in the body of the cuboctahedron.

TABLE III. Calculated ion separations and angles in the coordination polyhedron (8+1) of anions around the Ln ion in the hexameric cluster in fluorite-type crystals. The symbols are indicated in Fig. 6. In the antiprism, F_1 and F_2 anions form the square edges with the lengths a_1 and a_2, respectively.

Crystal	$\langle$Ln-$F_1\rangle$ (Å)	Θ_1 (deg)	$\langle$Ln-$F_2\rangle$ (Å)	Θ_2 (deg)	$\langle$Ln-$F_c\rangle$ (Å)	a_2 (Å)	b (Å)
CaF_2	2.41	54.6	2.28	107.2	2.85	3.08	2.07
SrF_2	2.44	53.9	2.31	108.9	2.93	3.09	2.19
BaF_2	2.47	52.9	2.35	110.9	3.03	3.10	2.33

takes on the value of X_α for the core and Y_α for the shell of the corresponding ions from Table II, and K_p^q are the numerical coefficients arising from the replacement of spherical harmonics by polynomials: $K_2^0=1/4$, $K_4^0=1/64$, $K_4^4=35/64$, $K_6^0=1/256$, and $K_6^4=63/256$.[42,45]

The exchange term is

$$B^q_{p\ s}=\frac{2(2p+1)}{7}K_p^q e^2 G\sum_\alpha S_p(r_\alpha)P_p^q(x_\alpha,y_\alpha,z_\alpha,r_\alpha)r_\alpha^{-(p+1)}, \tag{12}$$

where the summation α is carried out over the shells of the nearest fluorine ions, the exchange charge G is specific for Ln ions and ligands and is estimated as $G\sim 10$ for fluorite type crystals, and S_p are the bilinear forms constructed from the overlap integrals of the $4f$ wave functions of the Ln ion with $2s$ and $2p$ functions of the fluorine ions.[42,46] The dependence of S_p on the Ln^{3+}-F^- distance was calculated in Ref. 46 using Hartree functions of free ions. It can be fitted by the exponential

$$S_P(r_\alpha)=S_p^0\exp(-\delta_p r_\alpha). \tag{13}$$

Finally, the ECM parameters taken from Refs. 42 and 46 and used in this work are given in Table IV. Note that, for all the Ln ions studied, we assumed the same values of the G and σ_p parameters which were given in Ref. 42 for the simple Er^{3+} centers in CaF_2.

The exchange sum over the shells of the nearest-neighbor fluorine ions and the electrostatic sum over the cores and shells of all ions in the defected region were calculated by direct summation in Eqs. (12) and (11), respectively. The remaining part of the crystal was taken into account by the Ewald method.

The calculated CEF parameters for Ln ions in the "symmetric" hexameric cluster are given in Table V. They were used for finding the eigenstates and wave functions of Stark levels of Er^{3+}, Tm^{3+}, and Yb^{3+} ions. Calculated spectroscopic factors of the ground states of these ions in the hexameric clusters are given in Table I.

The calculations agree with the experiment. The spectroscopic splitting factors of the paramagnetic Ln ions were calculated to be strongly anisotropic: the factors $g_\parallel$ are close to the theoretical maximum limits and $g_\perp=0$. The main contribution to the axial crystal field in the clusters is described by the parameter $B_{20}=\alpha_2 B_2^0$, and B_2^0 appears to be negative (see Table V). For Er^{3+}, Tm^{3+}, and Yb^{3+} ions, the Stevens coefficient $\alpha_2>0$. The matrix elements of the spin operators O_2^0 are positive and have their maximum values for states with the maximum projections of integral angular momentum on the principal symmetry axis: $J_z=\pm J$. Therefore, the $|\pm J\rangle$ doublets make the main contribution to the wave functions of the ground states of the paramagnetic Ln ions in the clusters. The CEF parameters B_4^4 and B_6^4 (see Table V) allow for an admixture of states with other J_z. However, our calculations show that the g tensors remain strongly anisotropic for all the paramagnetic Ln ions in the hexameric clusters. For Tm^{3+} ion (which has an even number of $4f$ electrons), the nonzero values of the B_4^4 and B_6^4 CEF parameters result in $1-2$ cm^{-1} splitting of the ground doublet characterized by $|\pm J_z\rangle=|\pm 6\rangle$ (see Table I).

It is interesting to compare the calculation results for the CEF parameters of the hexameric cluster with those of the simple cubic and tetragonal centers, which we have obtained within the same approach (see Table V). For cubic centers, the CEF parameter B_2^0 is equal to zero. In the simple tetrag-

TABLE IV. ECM parameters for Ln ions (Refs. 42 and 46). $\sigma_2=0.558$, $\sigma_4=\sigma_6=0$,[b] and $G=7.6$.[b]

Ion	$\ln S_2{}^0$	$\ln S_4{}^0$	$\ln S_6{}^0$	δ_2[a]	δ_4[a]	δ_6[a]
Er^{3+}	0.654	0.087	−1.471	1.994	1.896	1.648
Tm^{3+}	0.524	−0.152	−1.729	1,991	1,881	1,641
Yb^{3+}	0.394	−0.391	−1.987	1.987	1.864	1.633

[a]In atomic units.

[b]Assumed for all Ln ions studied.

TABLE V. CEF parameters (in cm^{-1}) for Er^{3+} in the hexameric cluster and in the simple centers in CaF_2.

CEF parameter	Cubic center	Tetragonal center	Contracted square antiprism[a]	Hexameric cluster
$B_2{}^0$	0.0	49.9	−613.1	−487.3
$B_4{}^0$	−78.7	−48.8	−87.4	−57.1
$B_4{}^4$	−393.5	−352.9	0.0	710.5
$B_6{}^0$	29.7	29.8	17.8	14.7
$B_6{}^4$	−623.7	−449.4	0.0	−98.9

[a]For an idealized model of highly symmetric surrounding of the Ln ion in a contracted regular square antiprism with D_{4d} symmetry, we assumed that the length a_1 is equal to a_2. The length a_2 and height b are equal to those in the hexameric cluster. The Ln^{3+} ion is placed into the center of the antiprism (see Fig. 6).

onal center, the presence of the neighboring interstitial F^- ion makes $B_2^0>0$ and changes slightly the other CEF parameters with respect to the cubic center. The "off-axial" parameters B_4^4 and B_6^4 are large enough as compared with the "axial" B_4^0 and B_6^0. There are strict relationships $B_4^4=5B_4^0$ and $B_6^4=-21B_6^0$ for a cubic crystal field. This results in a significant mixing of the wave functions with different projections of the angular momentum and approaching in values of the factors $g_\parallel$ and $g_\perp$ of the ground states of both Er^{3+} and Yb^{3+} ions. The spectroscopic splitting factors for the simple Ln^{3+}-F^- tetragonal centers[1] in CaF_2 are $g_\parallel=7.780$ (7.781), $g_\perp=6.254$ (6.365) for Er^{3+} and $g_\parallel=2.423$ (2.812), $g_\perp=3.878$ (3.743) for Yb^{3+} (our calculated values are given in parentheses). For cubic centers,[1] $g=6.785$ (6.800) for Er^{3+} and $g=3.438$ (3.429) for Yb^{3+}. For simple Tm^{3+} centers, the ground states are isolated singlets and the EPR spectra are not observed.[1]

The peculiar features of CEF at the site of the Ln^{3+} ion in the hexameric cluster can be explained by examining only the nearest local environment (see Fig. 6 and Table III). Eight F^- ions form a distorted square antiprism with C_{4v} symmetry. It only slightly differs from a contracted regular square antiprism [in which the length a_1 would be equal to a_2 and the Ln^{3+} ion is placed into its center (see Fig. 6)] with a higher symmetry of D_{4d} having the eightfold rotation-inversion axis S_8. The CEF parameters for the D_{4d} square antiprism, which simulates the "real" antiprism in the hexameric cluster, are also given in Table V.

Harris and Furniss[47] found that the CEF in a square antiprism with D_{4d} symmetry is pure axial—i.e., all the off-axial CEF parameters $B_{pq}\equiv 0$ when $q\neq 0$. The corresponding crystal-field Hamiltonian for the Ln ion can be written in the form

$$H_{CF}=B_{20}O_2^0+B_{40}O_4^0+B_{60}O_6^0. \tag{14}$$

It should be noted that, for the other highly symmetrical coordination polyhedrons (e.g., for cube, octahedron, tetrahedron, etc.), there are off-axial parameters $B_{pq}\neq 0$ (with $q\neq 0$) which are greater than all the axial ones. This results in a strong admixture of wave functions characterized by different projections J_z of the angular momentum J. Due to the parent D_{4d} symmetry with the eightfold axis S_8 of a square antiprism, the wave functions characterized by different J_z projections are mixed only under distortion of the antiprism. It is noteworthy that, in a regular antiprism (with $a_1=a_2=b$; see Fig. 6), the parameter $B_2^0=0$. However, B_2^0 becomes negative and increases in its absolute value upon contraction of a regular antiprism, making $b<a_1,a_2$. In the hexameric cluster, due to a strong Coulomb attraction of the F_{12} cuboctahedron to the Ln_6 octahedron, the antiprism appears to be contracted and B_2^0 is negative.

We estimated the change in the CEF parameters at the site of the Ln ion as a result of a probable displacement of the F^- ion from the center of the hexameric cluster and also of a replacement of one of the Ln ions in the octahedron Ln_6 with A cation (see the Introduction). (In the calculations, the possible shift of ions in the cluster and neighboring ions was not taken into account.) The change of the spectroscopic splitting factors of the ground states of the paramagnetic Ln ions appeared to be of the same order of magnitude or less than is due to a distortion of a square antiprism in the hexameric cluster. Therefore, these calculations do not allow one to discriminate between the possible diversity of hexameric clusters observed in the EPR spectra of fluorite-related solid solutions.

VI. CONCLUSIONS

The EPR study of yttrofluorite-type solid solutions $(AF_2)_{1-y}(LnF_3)_y$ which contain Ln ions of the second half of rare-earth series and yttrium reveals only hexameric clusters therein, presumedly of Ln_6F_{37} type. The nearest local environment of Ln ions in clusters is a square antiprism of F^- ions. A square antiprism is closely related to the bicapped trigonal prismatic geometry occuring in the YF_3 structure, which is adopted in all the lanthanide trifluorides LnF_3 with Ln from Sm to Lu.[47,48]

The calculations of CEF parameters and spectroscopic factors of Er^{3+}, Tm^{3+}, and Yb^{3+} in hexameric clusters show that a square antiprism environment forms a strong axial crystalline electric field. It accounts for the high—approaching the theoretical limits—principal values of g tensors for these paramagnetic ions. It is noteworthy that the EPR spectra of Tm^{3+} have been observed only in a few compounds with a rather low crystal symmetry,[49,50] apparently, because of a "casually strong" axial crystalline electric field therein. However, for the square antiprism of anions as a local environment, the occurrence of a non-Kramers doublet $|\pm J\rangle$ in the ground state of Tm^{3+} (and Tb^{3+}) ions is quite possible not only in crystals, but even in a fluorozirconate glass.[47] There is a whole class of fluorite-related structures with square antiprisms of anions.[18] One of its representatives is KY_3F_{10} crystal with the splitting factors for the Er^{3+} ion[51] close to those measured in our work.

Our work (see also Ref. 26), as well as the electron diffraction study,[15] reveals the tendency of the clusters to coagulate into domains that, probably, have superstructural ordering.

However, in contrast to the superstructures, there are also "simple" cubic Ln^{3+} centers in the "undisturbed" regions of the fluorite lattice of the solid solutions, located outside clusters or their domains. With an increase in the concentration of LnF_3 above ~1 mol %, the EPR spectra of the cubic centers are appreciably broadened and even exhibit a pronounced structure,[52] which implies a complex pattern of the solid solutions under study.

Nonstoichiometric fluorite solid solutions are nonequilibrium. It is known that, in moderately concentrated solid solutions (<5 mol %), the balance between clusters and simple centers can be shifted by prolonged annealing of a sample at $T=600$ °C (a process in which the cluster concentration increases) or by its quenching from $T=900$ °C, thus substantially reducing the cluster concentration in favor of the simple centers. However, the solid solutions appear to modify at room temperature as well. We observed the EPR spectra of Tm^{3+} ions in clusters to become more complex in "aged" samples after 20 years of their storage. The number of different positions of Ln ions in clusters increased. It is

possibly due to the rearrangement of clusters, in which the penetration of oxygen ions into the fluorite lattice (see Sec. II) may also occur.[18,19]

Our work confirms the assumption of Bevan, Ness, and Taylor,[18] based on a crystal chemistry study, that the high-temperature disorded (cubic) α phase of nonstoichiometric fluorites is made up of clusters formed by six corner-sharing square antiprisms enclosing a cuboctahedron of anions. These clusters are "kaleidoscopically" incorporated within the fluorite matrix. The disorder in the arrangement of the clusters and also the presence of "split" atoms,[17–19] apparently, could explain the phenomena—namely, the two level systems[33,53] and boson peaks[54]—which are usually characteristic of glasses, but were also revealed in fluorite-related solid solutions.

ACKNOWLEDGMENTS

We are thankful to P. P. Fedorov for fruitful discussions, to V. A. Shustov for an x-ray study, and to I. I. Fazlizhanov for his help in EPR measurements on the Varian spectrometer. The work of A.E.N., A.Yu.Z., and M.Yu.O. was supported by the Russian Foundation for Basic Research, Project No. 04-02-16427, and by Grant No. REC-005 (EK-005-XI).

[1] *Crystals with the Fluorite Structure*, edited by W. Hayes (Claredon, Oxford, 1974).
[2] D. S. Moore and J. C. Wright, J. Chem. Phys. **74**, 1626 (1981).
[3] J. P. Laval, A. Mikou, and B. Frit, Solid State Ionics 28-**30**, 1300 (1988).
[4] J. P. Laval, A. Abaous, and B. Frit, J. Solid State Chem. **81**, 271 (1989).
[5] C. R. A. Catlow, A. V. Chadwick, and J. Corish, J. Solid State Chem. **48**, 65 (1983).
[6] C. R. A. Catlow, A. V. Chadwick, G. N. Greeves, and L. M. Moroney, Nature (London) **312**, 601 (1984).
[7] C. R. A. Catlow, A. V. Chadwick, J. Corish, L. M. Moroney, and A. N. O'Reilly, Phys. Rev. B **39**, 1897 (1989).
[8] C. R. A. Catlow, A. V. Chadwick, G. N. Jacobs, and S. H. Ong, Phys. Rev. B **25**, 6425 (1982).
[9] P. J. Bendall, C. R. A. Catlow, J. Corish, and P. W. M. Jacobs, J. Solid State Chem. **51**, 159 (1984).
[10] P. P. Fedorov, Butll. Soc. Catalana Cienc. Fis., Quim. Mat. **12**, 349 (1991).
[11] J. A. Archer, A. V. Chadwick, I. R. Jack, and B. Zegrini, Solid State Ionics 9-**10**, 505 (1983).
[12] A. K. Ivanov-Shits, N. I. Sorokin, P. P. Fedorov, and B. P. Sobolev, Solid State Ionics **31**, 253 (1989).
[13] G. G. Andeen, J. J. Fontanella, M. G. Wintersgill, P. J. Welcher, R. J. Kimble, and G. E. Matthews, J. Phys. C **14**, 3557 (1981).
[14] P. P. Fedorov, O. E. Izotova, V. B. Alexandrov, and B. P. Sobolev, J. Solid State Chem. **9**, 368 (1974).
[15] O. Greiss and J. M. Hashke, in *Handbook on the Physics and the Chemistry of Rare Earths*, edited by K. A. Gschneidner and L. R. Eiring (North-Holland, Amsterdam, 1982).
[16] B. P. Sobolev, *The Rare-Earth Trifluorides* (Institut d'Estudis Catalans, Barselona, 2001), pt. 2.
[17] D. J. M. Bevan, M. J. McCall, S. F. Ness, and M. R. Taylor, Eur. J. Solid State Inorg. Chem. **25**, 517 (1988).
[18] D. J. M. Bevan, S. F. Ness, and M. R. Taylor, Eur. J. Solid State Inorg. Chem. **25**, 527 (1988).
[19] D. J. M. Bevan, J. Strahle, and O. Greiss, J. Solid State Chem. **44**, 75 (1982).
[20] J. P. Laval, A. Abaous, B. Frit, and A. Le Bail, J. Solid State Chem. **85**, 133 (1990).
[21] E. Secemski and W. Low, J. Chem. Phys. **64**, 4240 (1976); J. M. O'Hare, T. P. Graham, and G. T. Johnston, *ibid.* **64**, 4242 (1976).
[22] Yu. K. Voron'ko, A. A. Kaminskii, and V. V. Osiko, Zh. Eksp. Teor. Fiz. **50**, 15 (1966) [Sov. Phys. JETP **23**, 10 (1966)].
[23] Yu. K. Voron'ko, V. V. Osiko, and I. A. Shcherbakov, Zh. Eksp. Teor. Fiz. **56**, 151 (1969) [Sov. Phys. JETP **29**, 86 (1969)].
[24] S. A. Kazanskii and A. I. Ryskin, Fiz. Tverd. Tela (S.-Peterburg) **44**, 1356 (2002) [Phys. Solid State **44**, 1415 (2002)].
[25] S. A. Kazanskii, Pis'ma Zh. Eksp. Teor. Fiz. **38**, 430 (1983) [JETP Lett. **38**, 521 (1983)].
[26] S. A. Kazanskii, Zh. Eksp. Teor. Fiz. **89**, 1258 (1985) [Sov. Phys. JETP **62**, 727 (1985)].
[27] B. P. Sobolev, A. M. Golubev, E. A. Krivandina, M. O. Marychev, E. V. Chuprunov, X. Alcobe, S. Gali, L. Pascual, R.-M. Rojas, and P. Herrero, Kristallografiya **47**, 237 (2002) [Crystallogr. Rep. **47**, 201 (2002)].
[28] S. N. Jasperson and S. E. Schnatterly, Rev. Sci. Instrum. **40**, 761 (1969).
[29] S. Geshwind, in *Electron Paramagnetic Resonance*, edited by S. Geshwind (Plenum, New York, 1972), p. 353.
[30] C. Kittel, *Introduction to Solid State Physics* (Wiley, New York, 1957).
[31] A. Abragam and B. Bleaney, *Electron Paramagnetic Resonance of Transition Ions* (Claredon Press, Oxford, 1970).
[32] V. F. Tarasov and G. S. Shakurov, Appl. Magn. Reson. **2**, 571 (1991).
[33] S. A. Kazanskii, Pis'ma Zh. Eksp. Teor. Fiz. **41**, 185 (1985) [JETP Lett. **41**, 224 (1985)].
[34] J. M. Griffith, Phys. Rev. **132**, 316 (1963).
[35] *Computer Simulation of Solids*, edited by C. R. A. Catlow and W. C. Mackrodt, Lecture Notes in Physics (Springer, New York, 1982).
[36] V. A. Chernyshev, A. D. Gorlov, A. A. Mekhonoshin, A. E. Nikiforov, A. I. Rokeakh, S. Y. Shashkin, and A. Y. Zaharov, Appl. Magn. Reson. **14**, 37 (1998).
[37] B. G. Dick and A. W. Overhauser, Phys. Rev. **112**, 90 (1958).
[38] A. D. Gorlov, V. A. Chernyshev, M. Yu. Ougrumov, and A. V. Abrosimov, Fiz. Tverd. Tela (S.-Peterburg) **47**, 1389 (2005) [Phys. Solid State (to be published)].
[39] A. D. Gorlov, V. B. Guseva, A. P. Potapov, and A. I. Rokeakh, Fiz. Tverd. Tela (S.-Peterburg) **43**, 456 (2001) [Phys. Solid State **43**, 473 (2001)]; A. I. Rokeakh, A. A. Mekhonoshin, N. V. Legkikh, and A. M. Batin, *ibid.* **37**, 3135 (1995) [**37**, 1728

(1995)].

[40] The lattice constants (in nm) of the fluorite crystals calculated with the model parameters used in this work are 0.544 (0.544) for CaF_2, 0.579 (0.578) for SrF_2, and 0.623 (0.617) for BaF_2; the actual values are given in parentheses (see Refs. 36 and 38 for details).

[41] S. A. Al'tshuler and B. M. Kozyrev, *Electron Paramagnetic Resonance in Compounds of Transitional Elements*, 2nd revised ed. (Wiley, New York, 1974).

[42] B. Z. Malkin, in *Spectroscopy of Solids Containing Rare-Earth Ions*, edited by A. A. Kaplyanskii and R. M. Macfarlane (North-Holland, Amsterdam, 1987), p. 13.

[43] B. Z. Malkin, Z. I. Ivanenko, and I. B. Aizenberg, Fiz. Tverd. Tela (Leningrad) **12**, 1873 (1970) [Sov. Phys. Solid State **12**, 1491 (1970)]

[44] R. P. Gupta, B. K. Rao, and S. K. Sen, Phys. Rev. A **3**, 545 (1971).

[45] L. A. Bumagina, B. N. Kazakov, B. Z. Malkin, and A. L. Stolov, Fiz. Tverd. Tela (Leningrad) **19**, 1073 (1977) [Sov. Phys. Solid State **19**, 624 (1977)].

[46] M. P. Davydova, B. N. Kazakov, and A. L. Stolov, Fiz. Tverd. Tela (Leningrad) **20**, 2391 (1978) [Sov. Phys. Solid State **20**, 1378 (1978)].

[47] E. A. Harris and D. Furniss, J. Phys.: Condens. Matter **3**, 1889 (1991).

[48] S. P. Vernon and M. B. Stearns, Phys. Rev. B **29**, 6968 (1984).

[49] I. E. Rouse and J. B. Gruber, Phys. Rev. B **13**, 3764 (1976).

[50] J. M. Baker, C. A. Hutchison, and P. M. Martineau, Proc. R. Soc. London, Ser. A **403**, 221 (1986).

[51] R. Yu. Abdulsabirov, A. V. Vinokurov, I. N. Kurkin, E. A. Pudovik, A. L. Stolov, and Sh. I. Yagudin, Opt. Spektrosk. **63**, 97 (1987) [Opt. Spectrosc. **63**, 55 (1987)].

[52] H. R. Asatryan (private communication).

[53] S. A. FitzGerald, A. J. Sievers, and J. A. Campbell, J. Phys.: Condens. Matter **13**, 2095 (2001); **13**, 2177 (2001).

[54] J. J. Tu and A. J. Sievers, Phys. Rev. B **66**, 094206 (2002).